SAND2020-10527J

Structure-Property relationships in Rare Earth Iridate Pyrochlores

Tina M. Nenoff,[1]* David X. Rademacher,[2] Mark A. Rodriguez,[3] Terry J. Garino,[3]
Tamilarasan Subramani,[5] Alexandra Navrotsky[6]

[1] *Material, Physical and Chemical Sciences Center,*
[2] *Nanoscale Sciences Dept.*
[3] *Materials Characterization and Performance Dept.*
Sandia National Laboratories, Albuquerque, NM 87185, USA

[5] *Peter A. Rock Thermochemistry Laboratory*
University of California, Davis, CA 95616, USA

[6] *School of Molecular Sciences*
Arizona State University, Tempe, AZ 85287, USA

*Corresponding author: tmnenof@sandia.gov

ABSTRACT

Herein is presented the synthesis and characterization of rare earth iridate pyrochlore ($RE_2Ir_2O_7$; RE = Y, Eu, Pr) crystalline powders. The $RE_2Ir_2O_7$ phases are synthesized by high temperature solid state synthesis methods. X-ray diffraction (XRD) and elemental analysis techniques are utilized to validate the synthesis, and enable structural comparisons between the analog phases. Trends indicate the lattice parameter contacts with decreasing ionic radius of the RE element, and a contraction of the RE-O bonds is evident that is inversely reflected in the slight expansion of the Ir-O bond distance from Pr to Y. Structure-property relationship studies were expanded to include drop calorimetry thermochemistry; it was used to study the heats of formation of each phase. The resulting enthalpy of formations indicate that the heats of formation ($\Delta H°_{f,ox}$) becomes less exothermic with decreasing ionic radius for RE = Pr and Eu. For RE = Y, the enthalpy of formation is more exothermic despite the ionic radius being smaller than for Pr and Eu.

Sandia National Laboratories is a multimission laboratory managed and operated by National Technology & Engineering Solutions of Sandia, LLC, a wholly owned subsidiary of Honeywell International Inc., for the U.S. Department of Energy's National Nuclear Security Administration under contract DE-NA0003525.

Introduction

There is current great interest in the topological quantum materials (TQM) because of unique topological properties. Specifically, much research has concentrated on Dirac and Weyl semimetals, such as pyrochlore iridates.[1] Pyrochlore iridates were the first predicted TQM to host Weyl fermions,[2] where novel quantum phases emerge due to the interplay of electron correlations and strong spin-orbit interactions. To date, only optical evidence of such Weyl semimetal states in a bulk crystal has been reported.[3] There is no published transport evidence in iridate thin-films. In order to fabricate them as pure phase epitaxial thin films, pure phase pellets need to be prepared as targets for pulsed-laser deposition (PLD) methods.[4] Epitaxial films can be prepared on substrates such as $Y:ZrO_2$ with tunable biaxial strains.

Iridate pyrochlores are described as Weyl fermions. They are readily synthesized in a sintered powder disk that can be utilized for thin film formations via pulsed laser deposition techniques. The pyrochlore iridates $RE_2Ir_2O_7$ (R = Y or rare-earth lanthanides) possess a unique combination of extended 5d orbitals, strong electronic correlations, small magnetic moments, geometric frustration, and large spin-orbit coupling effects. In the case of R = Pr, these features appear to give rise to a novel metallic spin liquid ground state and an anomalous Hall effect. When R = Eu, Y, Nd, Sm, Lu, these features have been predicted to give rise to new topological phases, such as the Weyl semimetal state.[5] $Y_2Ir_2O_7$ was predicted by DFT to be a class of topological Weyl semimetals exhibiting remarkable topological properties, and including the expected fermi arc surface states.[2]

Experimentally, there is optical evidence for a Weyl semimetal state was reported in the pyrochlore $Eu_2Ir_2O_7$,[6] and a magneto Hall effect was studied in extensive detail in pyrochlore iridates.[7] A spontaneous Hall effect was observed in an all-in all-out pyrochlore iridate, providing another important example of topological states in this system.[8]

Pyrochlores ($A_2B_2O_7$) are a family of compounds with a fluorite derived superstructure with ordered oxygen vacancies. Pyrochlores can accommodate a variety of cations in their structure thus resulting in wide range of natural and synthetic compositions.[9] Different cations induce interesting chemical and physical properties in these oxides leading to diverse applications.[10-12]

The goal of this study is to synthesize $RE_2Ir_2O_7$ pyrochlores via solid state synthesis under controlled oxidizing atmosphere for preparation in PLD use of thin film fabrication. Furthermore,

a systematic study of the changes in heats of formation of the analogs will help elucidate thermochemical differences in the phases. Herein, we report on the effect of RE cation selection on changes in crystal structure and enthalpies of formation ($\Delta H°_{f,ox}$) of iridium based $RE_2Ir_2O_7$ pyrochlores (see Figure 1), as determined by the high temperature oxide melt solution calorimetry. Structure-property relationships between the various members of this pyrochlore family are extrapolated.

Experimental Section

Synthesis of $Y_2Ir_2O_7$ crystalline powder. Amending a previously reported preparation method,[13] $Y_2Ir_2O_7$ is prepared via a solid state reaction process. Alfa Aesar Premion IrO_2 99.991.3540% and Fluka AG Y_2O_3 99.999% are mixed in 2:1 molar ratio (1.8585 g IrO_2 & 0.9036 g Y_2O_3). The powders are placed into the zirconia Spex Mill vial with 10ml of a binder made of saturated solution of Acros MW 95K PVA (Polyvinyl Alcohol) and DI H_2O. This mix is then Spex milled for 30 minutes, and then placed in a 105°C oven overnight to dry. The resultant powder is then pressed on a Carver C press to 10,000 lbs in a Carver 1" die. The resulting pellet is removed and placed inside a closed alumina crucible that is then placed itself inside a larger alumina crucible. This ensures minimal loss of the volatile iridate during heating. The powder pellet is fired at 1000°C for 72 hours, with a ramp up and down rate of 100°C/hour.

The phase purity of the resulting fired pellet is confirmed by powder XRD. After this initial round of heating, the sample consisted of primarily $Y_2Ir_2O_7$ and a small but identified fraction of unreacted Y_2O_3. Additional IrO_2 (0.2506 gm) to match the calculated excess Y molar amount. The sample is then re-Spex Milled with binder, dried and fired as above, for several more cycles (6 more cycles to be precise) When the residual Y_2O_3 is measured at ≈ 1% by XRD quantification, the processing is considered finished.

Synthesis of $Eu_2Ir_2O_7$ crystalline powder. Similar to the preparation above for $Y_2Ir_2O_7$, a mixture of Eu_2O_3 and IrO_2 are mixed together, ground in a Spec Mill, heated, ground, pressed into a pellet, reheated for time, and characterized for phase purity. In this experiment, 7.0 g of (Lindsay Chemical) Eu_2O_3 (0.0199 mol) was added to 8.920g Alfa Aesar IrO_2 (0.03978 mol) were mixed; an additional 10% excess IrO_2 was added to ensure adequate iridate remained in case of

volatilization during heating. The reactants are mixed with water and binder, heated overnight to dry at 105°C. The dried powder is pressed into a pellet at 5000 lbs in a 1 inch steel die and placed into a clean Pt crucible. This crucible was then placed into an Al_2O_3 crucible and covered with an Al_2O_3 lid, and it was further placed into a second Al_2O_3 crucible and covered with the lid. The assembly was repeated heated at temperatures up to 900°C for a total of 36 hours, followed by 72 hours. Powder XRD was run on the ground pellet in between each heating cycle to identify extent of phase purity. Due to excess IrO2 remaining, an additional 0.03 g of Eu_2O_3 (for a total of 1.05g Eu_2O_3) was added to the ground pellet, and re-Spex milled, binder added, pressed into a 1 inch pellet and heated to 900°C for 24 hours. The resultant $Eu_2Ir_2O_7$ phase was ~99% pure, with >1% IrO_2 impurity.

Synthesis of $Pr_2Ir_2O_7$ crystalline powder. Similar to the preparation above for $Eu_2Ir_2O_7$, a mixture of Lindsay Chemical Pr_6O_{11} (Not Available without ICP-MS) 6.8096g (0.0400 mol) and Alfa Aesar IrO_2 (99.99%) 9.0585g (0.0404 mol). A 1 mol% excess of Pr_6O_{11} is included in this mixture amount. The remainder of the process is a duplicate of the $Eu_2Ir_2O_7$ process detailed above.

Characterization techniques

A Siemens model D500 θ-θ powder diffractometer (Bruker AXS, Inc. Madison, WI) was used for standard powder XRD data collection with samples maintained at ambient temperature. Monochromatic Cu Kα (0.15406 nm) radiation was produced using a diffracted-beam curved graphite monochromator. Fixed slits were used, and the instrument power settings were 40 kV and 30 mA. Datascan V4.3 (Materials Data Inc.; Livermore, CA) software was used to operate the diffractometer. The condition for the XRD scan was as follows: 5-80° 2θ range, step-size of 0.04° 2θ and a count time of 4 seconds per step. Phase identification was performed using Jade 9.6 software package (Materials Data, Inc. Livermore, CA) coupled with the 2018 Powder Diffraction File - PDF4+ (ICDD, Newtown Square, PA). Reitveld refinement on powder crystalline X-ray diffraction patterns for the three samples was performed using GSAS II software package.[14-15]

X-ray Fluorescence was performed using a Bruker M4 Tornado Micro-X-ray Fluorescence system (Bruker AXS, Inc. Madison, WI). Spatial Mapping was performed using the M4 Tornado v1.3 software.

Energy dispersive spectroscopy (EDS) and scanning electron microscopy (SEM) data were collected on a JEOL JMS-6300V scanning electron microscope with the LINK GEM light-window energy dispersive spectrometer. Energy-dispersive X-ray spectroscopy (EDAX) was performed during SEM analysis, using an accelerating voltage of 10 kV and working distance of 10.9 mm and a Bruker XFlash 6 | 60 EDS detector.

High temperature oxide melt solution calorimetry

High temperature oxide melt solution calorimetry experiments for all the samples were done in a custom built Tian-Calvet twin calorimeter.[16-19] About 5-10 mg of pelletized samples were dropped from room temperature into molten sodium molybdate ($3Na_2O•4MoO_3$) solvent in a silica glass crucible at 973 K. The calorimetry setup was flushed by oxygen gas at a flow rate of 30 mL/min. The solvent was bubbled with the same gas at a flow rate of 5 mL/min throughout each experiment to avoid the reduction of IrO_2 at high temperature and facilitate the dissolution. At least 6-8 experiments were done per sample and the results report are average values with error being two standard deviations of the mean. The calorimeter was calibrated using the heat content of 5 mg pellets of α-Al_2O_3.

Results and Discussion

Phase identification and confirmation of the three RE iridate pyrochlores were performed by a combination of powder X-ray diffraction, SEM-EDS and elemental analysis (micro-XRF). The rare earth (RE) iridate phases crystalize in the cubic space group *Fd-3m* (No. 227, origin choice 2),[20] with the RE (Y, Pr, Eu), Ir, O1, and O2 atoms occupying the 16c, 16d, 48f, and 8b Wyckoff symmetry sites, respectively. As shown in Figure 1, each Ir atom resides in the center of an IrO6 octahedra. It is then hexagonally surrounded by the A cation (Y, Eu or Pr).

$Y_2Ir_2O_7$. The product is a black sintered disk, 1" in diameter (see Supporting Information, SI, Figure 1). SEM-EDS indicated a mixture of grain sizes, with only the expected Y, Ir and O signals present in the EDS.

$Eu_2Ir_2O_7$. The product is a black sintered disk, 1" in diameter. SEM-EDS indicated a wide range mixture of distinct particle sizes, with only the expected Eu, Ir and O signals present in the EDS. (atomic ratios O 66, Eu 18, Ir15%). See SI Figure 2.

$Pr_2Ir_2O_7$. The product is a black sintered disk, 1" in diameter. SEM-EDS indicated a mixture of sintered particle sizes, with only the expected Pr, Ir and O signals present in the EDS. (atomic ratios O 63, Pr 19, Ir18%). See SI Figure 3.

Structural Analysis.

Phase identification and Rietveld structure refinement were performed on the $Y_2Ir_2O_7$, $Eu_2Ir_2O_7$, and $Pr_2Ir_2O_7$ samples. See Figures 2-4. While the $Y_2Ir_2O_7$ sample proved to be a phase-pure pyrochlore structure, the $Eu_2Ir_2O_7$, and $Pr_2Ir_2O_7$ were mixed phase where the $Eu_2Ir_2O_7$ showed pyrochlore with a trace of IrO_2 and the $Pr_2Ir_2O_7$ showed the pyrochlore along with minor phases of both IrO_2 and Pr_3IrO_7; significant sample displacement correction was required in these two phases. Occluded IrO_2 was used as a reference phase.

Even though the Eu and Pr pyrochlores were not phase pure, it was still possible to extract structural parameters from the XRD patterns due to knowledge of all the observed structures (including impurity phases) as well the relative simplicity of the pyrochlore structure (cubic *Fd-3m,* 90°) with only two structural parameters, namely the single value for the lattice parameter (a-axis) and the oxygen *x* position in the lattice. All other atom *xyz* parameters are fixed by symmetry. For the three syntheses analyzed, the Pr^{+3} represents the largest radius of the pyrochlore series, whereas Y, while not explicitly a RE metal, represents the smallest ionic radius.

Eu represents an intermediate ionic radius between Pr and Y. Furthermore, it is important to remember that the trivalent lanthanides, such as Pr and Eu, exhibit a traction of their ionic radii due to the increased shielding by their 4f-electrons.[21] The $Eu_2Ir_2O_7$ pyrochlore structure has a cell volume of 1088.5 $Å^3$ and falls, as expected, between Y and Pr due to atomic radii ordering. Interestingly, the changes in the Ir-O-Ir bond angle has been shown to affect the phases' electronic behaviors.[13] With these pyrochlores this specific bond angle follows the following trend: around O1, the O1-Ir-O1 bond angle decreases from Y to Pr, but is compensated by the Ir-O1-Ir bond angle slightly increasing from Y to Pr.

As shown in Table 1, the lattice parameter contacts with decreasing ionic radius of the rare earth element. The variation of the cell dimension combined with the refined oxygen position in the lattice dictate the bond length values. The bonding behavior is also consistent with RE atomic radius, where the oxygen position within the structure responds to the decreased RE ionic size by exhibiting bond-length contraction for the RE-O bonds from Pr to Eu, and then to Y. This contraction of the RE-O bonds is inversely reflected in the slight, but detectable, expansion of the Ir-O bond distance from Pr to Y (see Table 2).

Calorimetry. The drop solution enthalpy (ΔH_{ds}) of IrO_2 is determined in this work to be 42.63 ± 1.63 kJ/mol. The drop solution enthalpies (ΔH_{ds}) and the enthalpies of formation from oxides ($\Delta H°_{f,ox}$) of $RE_2Ir_2O_7$ (RE = Pr, Eu, Y) are given in the Table 3. The thermochemical cycle used to calculate the enthalpies of formation from oxides is given in Table 4. Figure 5 shows enthalpy of formation from oxides, $\Delta H°_{f,ox}$, vs ionic radius. The enthalpies of formation of all compounds show that these materials are stable with respect to their component oxides.

It has been observed in the literature that there is a non-metal change over in pyrochlore iridates when the A cation is substituted along the rare-earth elements.[22] In particular, the smaller diameter ions such as Gd through Yb, exhibit non-metallic behavior. Contrary to this are the larger diameter ions including Pr through Eu. This change over is directly tied to the electron correlation among the Ir 5d electrons with the A site cations in these geometrically frustrated phase systems. Interest in possible correlations between the metallic change over, and the structural substitutions led to this study of the A cation atomic radii with internal local phase distortions, and the thermochemistry (heats of formation) associated with the different analogs. As such three A cation substitution analog phases were targeted: Pr (metallic lanthanide), Eu (nonmetallic lanthanide), and Y (rare earth).

This oxide pyrochlore family is of particular interest due to the spin-orbit coupling and geometric frustration associated with their electronic and ionic properties. Therefore, expanding the structure-property relationship understanding is a focus of this work. It is in this scope that three representative phase analogs were synthesized, characterized and utilized in thermochemical studies. The resulting enthalpy of formations indicate that the heats of formation ($\Delta H°_{f,ox}$) becomes less exothermic with decreasing ionic radius for RE = Pr and Eu as observed in other $RE_2M_2O_7$ (M = Ti, Zr and Sn) pyrochlores.[23-25] For RE = Y, the enthalpy of formation is more exothermic

despite the ionic radius being smaller than for Pr and Eu. The metallic and non-metallic nature of the compounds might be the reason for such behavior.

Conclusion

Herein is presented the synthesis and characterization of rare earth iridate pyrochlore ($RE_2Ir_2O_7$; RE = Y, Eu, Pr) crystalline powders. Because pyrochlore iridates have been predicted as topological quantum materials that might host Weyl fermions, where novel quantum phases emerge due to the interplay of electron correlations and strong spin-orbit interactions.[1,26,27] The need for experimental studies has led to the effort in synthesizing iridate thin-films. In order to fabricate them as pure phase epitaxial thin films, pure phase pellets need to be prepared as targets for PLD methods. Herein, efforts have focused on both the synthesis of the $RE_2Ir_2O_7$ phases and the elucidation of additional structure-property relationships that might exist in variations of the analogs.

Learning and leveraging from the success of these literature reports, a successful method of synthesizing and fully characterizing $RE_2Ir_2O_7$ (RE = Y, Eu, Pr) is presented. Powder X-ray diffraction and Reitveld refinements enabled structural comparisons between the analogs. Trends indicate that the lattice parameter contacts with decreasing ionic radius of the RE element. Furthermore, a contraction of the RE-O bonds is evident that is inversely reflected in the slight expansion of the Ir-O bond distance from Pr to Y. Drop solution calorimetry enabled the determination of the heats of formation of the various analog phases and aided in describing the differences between the metallic and nonmetallic members of this family of materials. The resulting enthalpy of formations indicate that the heats of formation ($\Delta H°_{f,ox}$) becomes less exothermic with decreasing ionic radius for RE = Pr and Eu. For RE = Y, the enthalpy of formation is more exothermic despite the ionic radius being smaller than for Pr and Eu.

The direct correlation between the changes in lattice constants, key bond lengths or oxygen atoms 1 and 4 around the cation, changes in framework unit cell and calorimetry results indicate that there is no overall change in the crystal structure for the $A_2Ir_2O_7$ pyrochlores studied here. There are, however, localized changes in the structure that accommodate for the size of the A^{3+} cation that affect the thermochemical nature of the phase: decrease in RE-O bond lengths while a simultaneous expansion of the Ir-O bond distance from Pr to Eu and then to Y. Correlated with the thermochemistry, the heats of formation of the metallic (Pr) and rare earth (Y) iridate pyrochlores

are lower than for the nonmetallic $Eu_2Ir_2O_7$ analog. With the presence of unpaired f-electrons in its valence shell, Eu is paramagnetic but in general chemically reacts like a typical RE element. However, combining its ionic radius size with the constraints of the iridate pyrochlore structure, the Eu analog is shown here to be a thermodynamically less favorable phase of the three studied. Correlating the valence electrons, with the thermodynamic and structural data, lends evidence to instability playing a role at the metallic/nonmetallic transition of rare earth iridate pyrochlores.

Acknowledgements

The authors thank Dr. Susan Henkelis for help with graphics, and Dr. Wei Pan and Dr. Jon Ihlefeld for helpful discussions. This work is supported by the Laboratory Directed Research and Development Program at Sandia National Laboratories. Sandia National Laboratories is a multi-mission laboratory managed and operated by National Technology and Engineering Solutions of Sandia, LLC., a wholly-owned subsidiary of Honeywell International, Inc., for the U.S. Department of Energy's National Nuclear Security Administration under contract DE-NA0003525. This paper describes objective technical results and analysis. Any subjective views or opinions that might be expressed in the paper do not necessarily represent the views of the U.S. Department of Energy or the United States Government.

References

1. Lee, S.R.; Sharma, P. A.; Pan, W.; Lima-Sharma, A.L.; Nenoff. T.M. Topological quantum materials for realizing Majorana quasiparticles, *Chem. Mater.* **2019**, *31*, 26-51.
2. Wan, X.; Turner, A.M.; Vishwanath, A.; Savrasov, S.Y. Topological semimetal and Fermi-arc surface states in the electronic structure of pyrochlore iridates, *Phys. Rev. B* **2001,** *83,* 205101.
3. Sushkov, A.B., Hofmann, J.B.; Jenkins, G.S.; Ishikawa, J.; Nakatsuji, S.; Das Sarma, S.; Drew, H.D. Optical evidence for a Weyl semimetal states in pyrochlore $Eu_2Ir_2O_7$, *Phys. Rev. B* **2015***, 92,* 241108(R).
4. Fujita, T.C., Kozuka, Y.; Uchida, M; Tsukazaki, A.; Arima, T; Kawasaki, M. Odd-parity magnetoresistance in pyrochlore iridate thin films with broken time-reversal symmetry, *Scientific Reports,* **2015***, 5.*
5. Clancy, J. P.; Gretarsson, H.; Lee, E.K.H.; Tian, D.; Kim, J.; Upton, M. H.; Casa, D.; Gog, T.; Islam, Z.; Jeon, B-G.; Kim, K. H.; Desgreniers, S.; Kim, Y. B.; Julian, S. J.; Kim, Y.-J. X-ray scattering study of pyrochlore iridates: Crystal structure, electronic, and magnetic excitations. *Phys. Rev. B.* **2016**, *94*, 024408.
6. Sushkov, A. B.; Hofmann, J. B.; Jenkins, G. S.; Ishikawa, J.; Nakatsuji, S.; Das Sarma, S.; Drew, H. D. Optical evidence for a Weyl semimetal state in pyrochlore $Eu_2Ir_2O_7$. *Phys. Rev. B* **2015**, *92*, 241108, DOI: 10.1103/PhysRevB.92.241108.
7. Ueda, K.; Oh, T.; Yang, B-J.; Kaneko, R.; Fukioka, J. Nagaosa, N.; Tokura, Y. Magnetic-Field induced multiple topological phases in pyrochlore iridates with Mott criticality. *Nat. Commun*. **2017**, *8*, 15515, DOI: 10.1038/ ncomms15515.
8. Ueda, K.; Kaenko, R.; Ishizuka, H.; Fujioka, J.; Nagaosa, N; Tokura, Y. Spontaneous Hall Effect in the Weyl semimetal candidate of all-in all-out pyrochlore iridate. *Nat. Commun*. **2018**, *9*, 3032, DOI: 10.1038/s41467-018-05530-9.
9. Subramanian, M. A.; Aravamudan, G.; Subba Rao, G. V. Oxide pyrochlores — A review, *Prog. Solid State Chem.*, **1983**, *15*, 55-143.
10. Gardner, J. S.; Gingras, M. J. P.; Greedan, J. E. Magnetic pyrochlore oxides, *Rev. Mod. Phys.*, **2010**, *82*, 53-107.

11. Zeng, J.; Wang, H.; Zhang, Y. C.; Zhu, M. K.; Yan, H. Hydrothermal synthesis and photocatalytic properties of pyrochlore $La_2Sn_2O_7$ nanocubes, *J. Phys. Chem. C*, **2007**, *111*, 11879-11887.
12. Ewing, R. C.; Weber, W. J.; Lian, J. Nuclear waste disposal—pyrochlore ($A_2B_2O_7$): Nuclear waste form for the immobilization of plutonium and "minor" actinides, *J. Appl. Phys.*, **2004**, *95*, 5949-5971.
13. Shapiro, M. C.; Riggs, S. C.; Stone, M. B.; de la Cruz, C. R.; Chi, S.; Podlesnyak, A. A.; Fisher, I.R. Structure and magnetic properties of the pyrochlore iridate $Y_2Ir_2O_7$. *Phys. Rev. B* **2012**, *85*, 214434.
14. Larson, A. C., and Von Dreele, R. B. (**2000**). *General Structure Analysis System (GSAS)* (Los Alamos National Laboratory Report LAUR 86-748).
15. Toby, B. H. (**2001**). "EXPGUI, a graphical user interface for GSAS," *J. Appl. Crystallogr.* **34**, 210-221.
16. Navrotsky, A. Progress and new directions in calorimetry: A 2014 perspective, *J. Am. Ceram. Soc.*, **2014**, *97*, 3349-3359.
17. Navrotsky, A. Mineralogy, materials science, energy, and environment: A 2015 perspective. *Am. Mineral.* **2015**, 100, 674-680.
18. Navrotsky, A. Progress and new directions in high temperature calorimetry. *Phys. Chem. Miner.* **1977**, 2, 89-104.
19. Navrotsky, A. Progress and new directions in high temperature calorimetry revisited. *Phys. Chem. Miner.* **1997**, 24, 222–241.
20. Millican, J.N.; Macaluso, R. T.; Nakatsuji, S.; Machida, Y.; Maeno, Y.; Chan, J. Y. Crystal growth and structure of $R_2Ir_2O_7$ (R=Pr, Eu) using molten KF. *Mater. Res. Bull.* **2007**, *42*, 928-934.
21. Vogel, D.J, Nenoff, T.M. Rimsza, J.M. "Tuned Hydrogen Bonding in Rare Earth MOFs for Design of Optical and Electronic Properties", *ACS Applied Materials & Interfaces*, **2020**, *12*(4), 4531-4539.
22. Yanagishima, D.; Maeno, Y. Metal-Nonmetal Changeover in Pyrochlore Iridates. *J. Phys. Soc. Jpn.* **2001**, *70*, 2880-2883.
23. Helean, K. B.; Ushakov, S. V.; Brown, C. E.; Navrotsky, A.; Lian, J.; Ewing, R. C.; Farmer, J. M.; Boatner, L. A. Formation enthalpies of rare earth titanate pyrochlores, *J. Solid State Chem.*, **2004**, *177*, 1858-1866.

24. Lamb, E.; Donnelly, R. G. ORNL isotopic power fuels quarterly report for period ending June 30, 1973. No. ORNL-4174, Oak Ridge National Lab., Tenn. (USA), Oak Ridge National Lab., Tenn. (USA), 1973.
25. Lian, J.; Helean, K. B.; Kennedy, B. J.; Wang, L. M.; Navrotsky, A.; Ewing, R. C. Effect of structure and thermodynamic stability on the response of lanthanide stannate pyrochlores to ion beam irradiation, *J. Phys. Chem. B*, **2006**, *110*, 2343-2350.
26. Nenoff, T.M.; Rademacher, D. X.; Rodriguez, M. A. Pan, W. Single Crystal Synthesis and Characterization of Cu intercalated $ZrTe_5$, *Crystal Growth & Design*, **2020**, *20*(2), 699-705.
27. Yu; W. Elias; J. A.; Chen, K-W.; Baumbach, R.; Nenoff, T. M.; Modine, N. A.; Pan, W.; Henriksen, E. A. Electronic transport properties of a lithium-decorated $ZrTe_5$ thin film, *Sci. Reports.* **2020**, *10,* 3537. DOI: 10.1038/s41598-020-60545-x

Tables.

Table 1. Refined crystallographic variations in $RE_2Ir_2O_7$ (RE = Y, Eu, Pr) phases.

Sample	a (Å)	Volume (Å^3)	O1 (*x*)
$Y_2Ir_2O_7$	10.1696(2)	1051.7	0.3475(8)
$Eu_2Ir_2O_7$	10.2867(6)	1088.5	0.341(1)
$Pr_2Ir_2O_7$	10.3561(2)	1110.7	0.337(1)

Table 2: Bond distance and angles for $RE_2Ir_2O_7$ Pyrochlores

Bond or Angle	$Y_2Ir_2O_7$	$Eu_2Ir_2O_7$	$Pr_2Ir_2O_7$
Ir-O1 (Å)	2.053(4)	2.045(6)	2.041(5)
RE-O1 (Å)	2.374(5)	2.447(9)	2.489(8)
RE-O2 (Å)	2.202(1)	2.227(1)	2.242(1)
RE-O2-RE (°)	109.47(1)	109.47(1)	109.47(1)
O1-Ir-O1 (°)	102.4(2) 77.6(2)	100.3(4) 79.6(4)	99.1(4) 80.9(4)
Ir-O1-Ir (°)	122.2(4)	125.6(7)	127.5(6)

Table 3. The drop solution enthalpies (Δds) and the enthalpies of formation from oxides ($\Delta H°_{f,ox}$) of $RE_2Ir_2O_7$ (RE = Pr, Gd, Y)

$RE_2Ir_2O_7$	**ΔH_{ds}(kJ/mol)**	**$\Delta H°_{f,ox}$(kJ/mol)**
$Pr_2Ir_2O_7$	-22.90±1.69(6)*	-83.28±8.92
$Eu_2Ir_2O_7$	12.12±0.60(6)	-55.06±3.80
$Y_2Ir_2O_7$	133.20±1.42(7)	-167.64±4.68

*The number of experiments carried out is given in the parenthesis ( ).

Table 4. Thermochemical cycle for the calculation of enthalpy of formation for $RE_2Ir_2O_7$ in $3Na_2O.4MoO_3$ solvent at 973 K with oxygen flushing

Reaction		**ΔH (kJ/mol)**
$RE_2Ir_2O_{7(s,298)} \rightarrow RE_2O_{3(sln,973)} + 2IrO_{2(sln,973)}$	[1] $\Delta H_{ds} - RE_2Ir_2O_7$	Table1[a]
$RE_2O_{3(s,298)} \rightarrow RE_2O_{3(sln,973)}$	[2] $\Delta H_{ds} - RE_2O_3$	Ref. 5[b]
$IrO_{2(s,298)} \rightarrow IrO_{2(sln,973)}$	[3] $\Delta H_{ds} - IrO_2$	43.15±1.55 (8)[c]
$RE_2O_{3(s,298)} + 2IrO_{2(s,298)} \rightarrow RE_2Ir_2O_{7(s,298)}$	[4] $\Delta H°_{f,ox} - RE_2Ir_2O_7$	Table1
$\Delta H[4] = -\Delta H[1]+\Delta H[2]+2\times\Delta H[3]$		

[a]Thermochemical cycle used to calculate the corrected enthalpy of drop solution for $Y_2Ir_2O_7$ is given in Appendix Table 1.

[b]Thermochemical cycle used to calculate the enthalpy of drop solution of Pr_2O_3 is given in Appendix Table 2.

[c]Measured in this work. The number of experiments carried out is given in the parentheses ( ).

Figures.

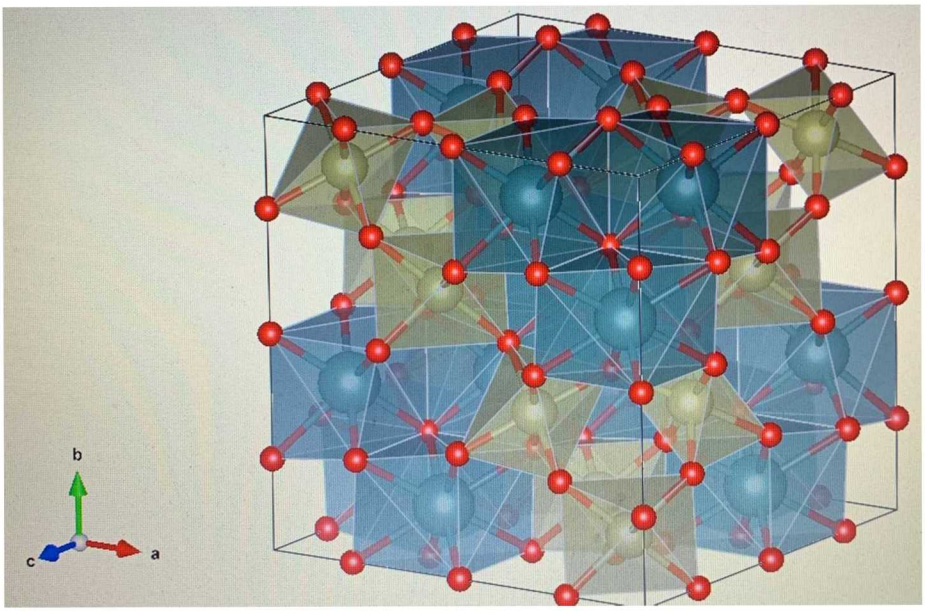

Figure 1. Crystal structure of $RE_2Ir_2O_7$, RE atoms in blue, Ir atoms in beige and Oxygen atoms in red. Space group Fd-3m, # 227.

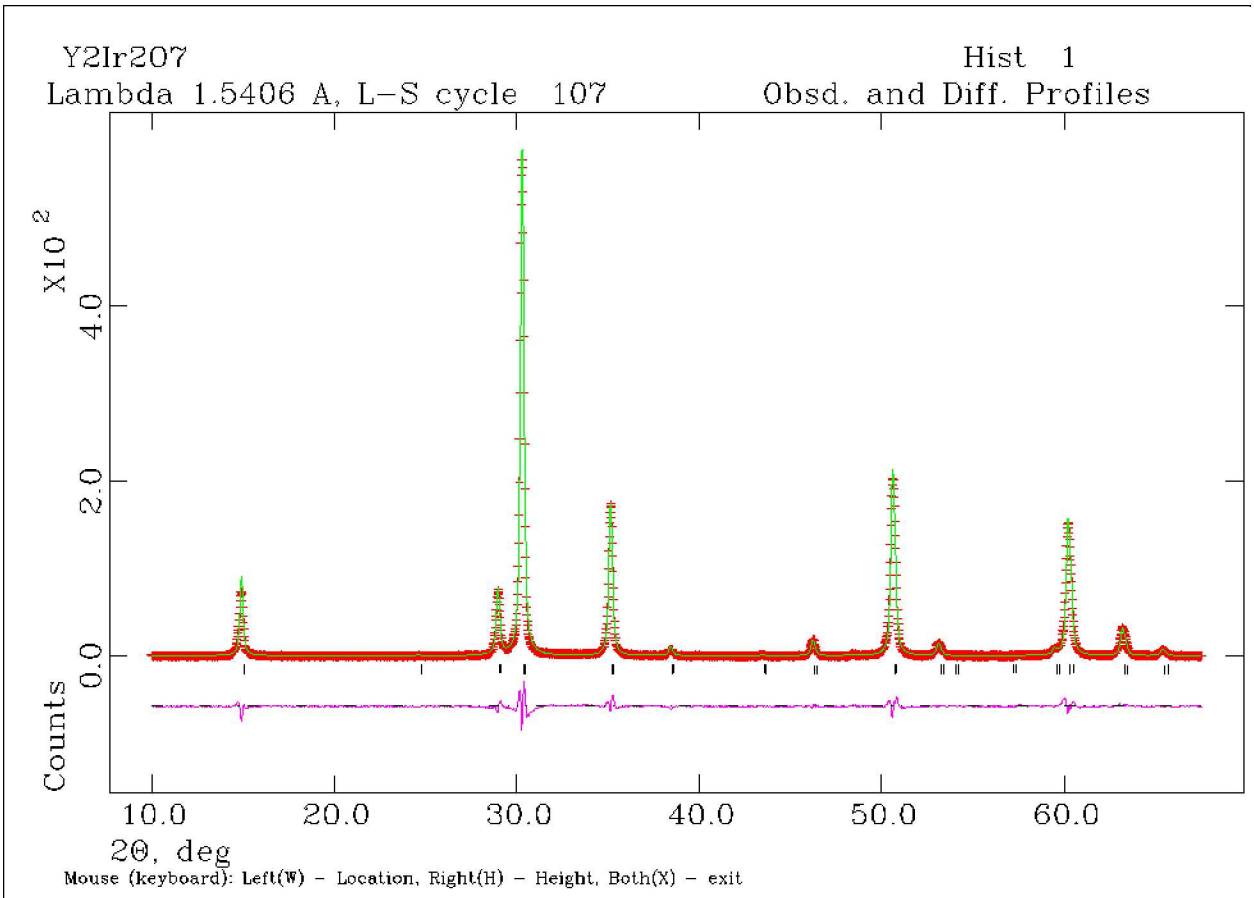

Figure 2. $Y_2Ir_2O_7$, X-ray powder diffraction pattern and GSAS Reitveld refinement fit, R_p = 8.38 %, R_{wp} = 11.05%. 100% pure phase.

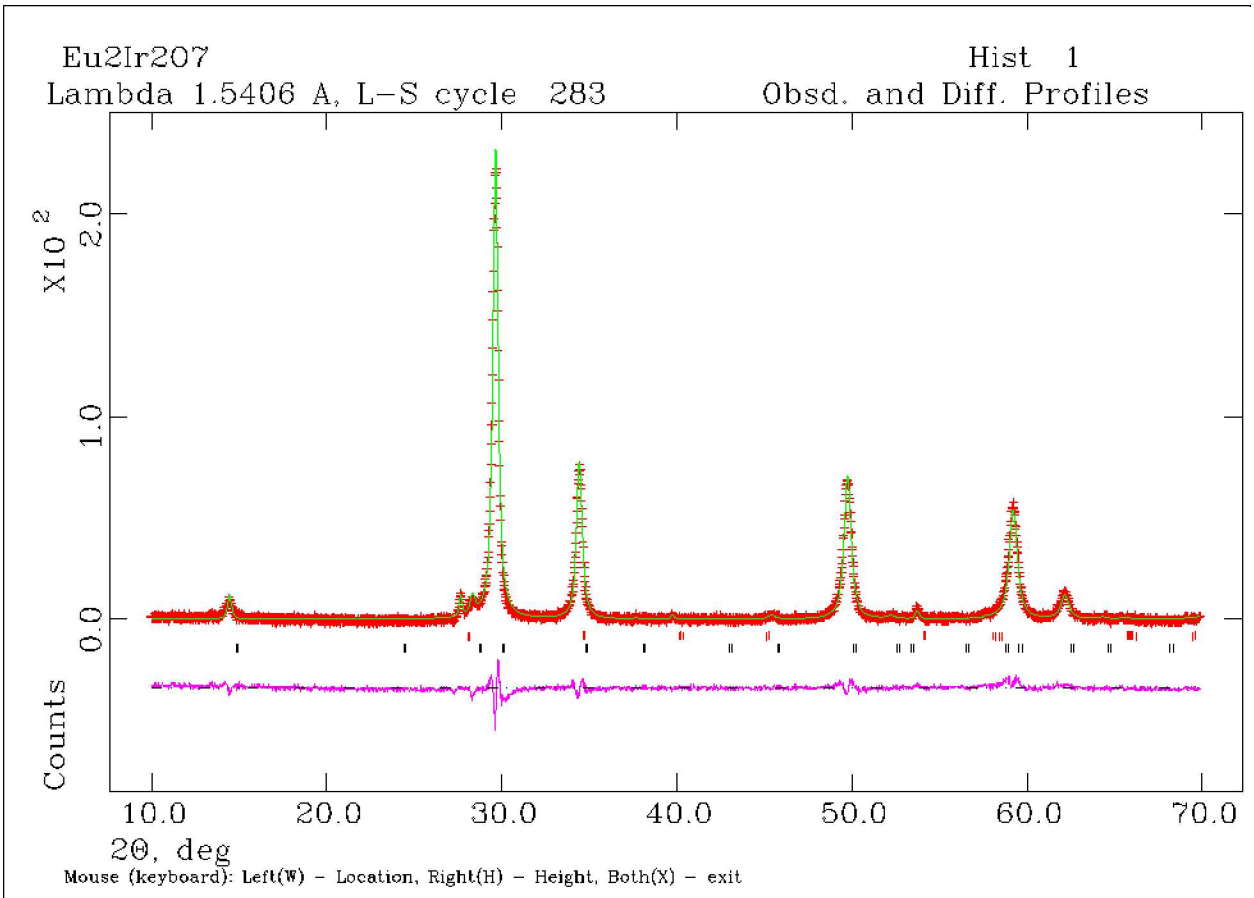

Figure 3. $Eu_2Ir_2O_7$, X-ray powder diffraction pattern and GSAS Reitveld refinement fit, R_p = 5.74%, R_{wp} = 7.26%. Phase composition: Eu pyrochlore = 97.3(1) wt.%, IrO_2 = 2.7(1) wt.%.

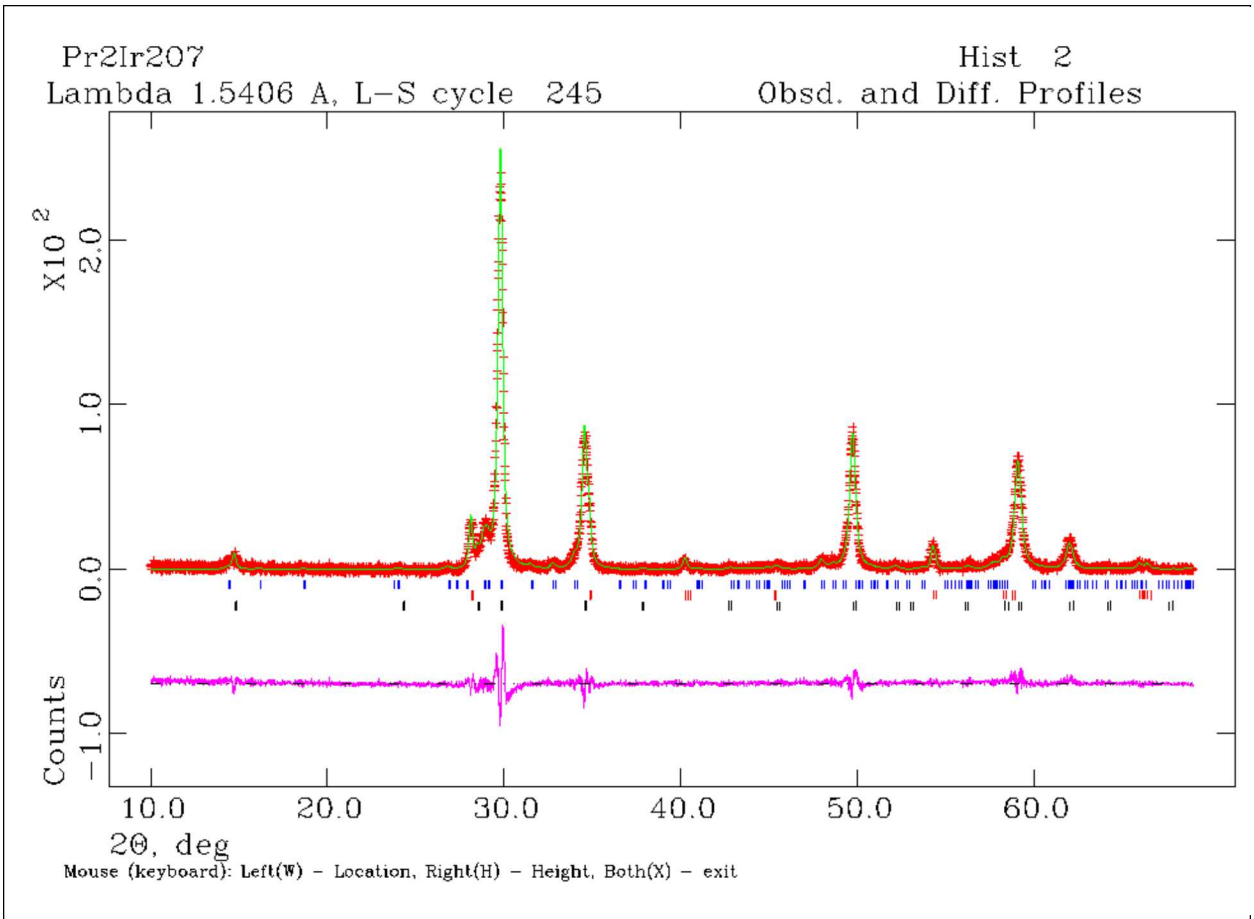

Figure 4. $Pr_2Ir_2O_7$, X-ray powder diffraction pattern and GSAS Reitveld refinement fit, R_p = 12.19%, R_{wp} = 15.91%. Phase composition: $Pr_2Ir_2O_7$ = 79.7(5) wt.%, IrO_2 = 8.4(1) wt.%, and Pr_3IrO_7 =11.9(2) wt.% in product mixture.

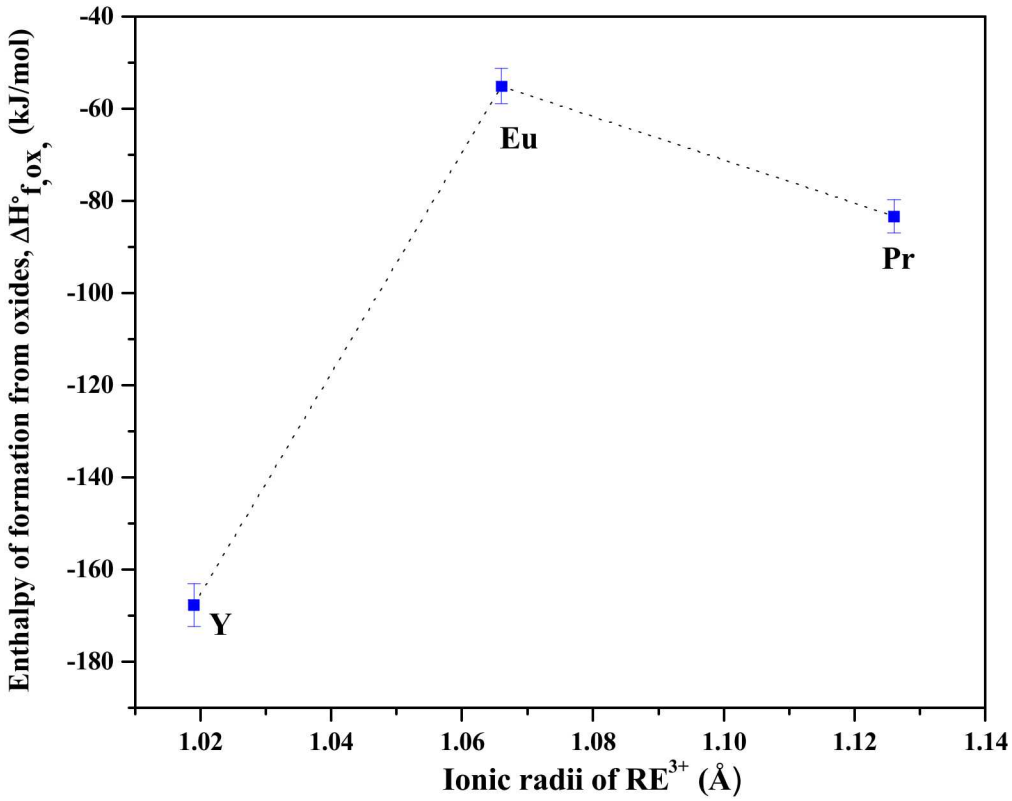

Figure 5: Enthalpy of formation from oxides, $\Delta H^{\circ}_{f,ox}$, vs ionic radius of RE^{3+}